

Electron energy levels for a dense electron gas in parabolic GaAs/Al_xGa_{1-x}As quantum wells

A. J. Rimberg and R. M. Westervelt

Department of Physics and Division of Applied Sciences, Harvard University, Cambridge, Massachusetts 02138

(Received 27 March 1989)

Parabolic GaAs/Al_xGa_{1-x}As quantum-well structures have been developed as a means of producing a uniform three-dimensional electron gas. Calculations of the actual density profile and energy levels in the Hohenberg-Kohn-Sham local-density-functional approximation are presented for several values of electron sheet density in the well. These results verify the predicted uniformity of the electronic-charge-density distribution over the occupied portion of the well and give more quantitatively correct estimates of the Fermi level and subband energy separations than available previously.

I. INTRODUCTION

Recent interest in the properties of high-mobility three-dimensional (3D) electron gas in strong magnetic fields¹ has led to the development of a novel structure, the remotely doped parabolic quantum well.² Using classical electrostatics and simple quantum-mechanical principles, approximate properties of the electron gas in such wells can be predicted:²⁻⁵ e.g., that the gas is roughly uniform across a width proportional to the electron sheet density n_s in the well; that the Fermi level is roughly independent of n_s , once more than one subband is occupied; and that the subband energy separations fall off approximately as $1/n_s^2$ when a large number of electrons are present. While experimental investigations of these structures have been made³⁻⁶ which are consistent with the above predictions, to date no detailed self-consistent calculations of the electronic energy levels and wave functions have been presented. The results presented here verify that the behavior predicted by simple arguments does occur and provide a quantitative determination of such experimentally important quantities as the Fermi level, subband energy separations, and number of occupied subbands, as functions of the number of electrons in the well.

In Sec. II we describe the physical structure of an actual parabolic well,² present the model used in these calculations, and discuss the method of calculation itself, which is similar to one used for GaAs/Al_xGa_{1-x}As heterojunctions.⁷ Section III gives the results of our calculations, and Sec. IV presents our conclusions.

II. METHOD OF CALCULATION

A typical (truncated) parabolic quantum well is illustrated schematically in Fig. 1(a). As described by Sundaram *et al.*² the wells are made by molecular-beam epitaxy and consist of GaAs and Al_{0.3}Ga_{0.7}As buffer layers on a GaAs substrate, followed by a Si-doped Al_{0.3}Ga_{0.7}As donor layer, an Al_{0.3}Ga_{0.7}As setback, and the parabolic well proper. On the other side of the well are a symmetrically placed setback and donor layer, an Al_{0.3}Ga_{0.7}As buffer, and a GaAs cap. The setbacks serve to separate

the donor ions from the electron gas and hence reduce ionized-impurity scattering. The well itself consists of a fine superlattice of 20-Å period in which the relative width of GaAs and Al_{0.3}Ga_{0.7}As layers in each period is computer controlled to produce an average Al concentration varying quadratically from $x=0$ at the well center to $x=0.2$ at the edge. The well is characterized by three parameters shown in Fig. 1(a): the height Δ_1 and width w of the parabola and the height Δ_2 of the Al_{0.3}Ga_{0.7}As barrier. Representative values of these parameters^{4,5} for a wide remotely doped parabolic well are $\Delta_1=155$ meV, $\Delta_2=75$ meV, and $w=4000$ Å.

In a semiclassical picture, where the wavelike nature of electrons is ignored, the parabolic-well concept² is based on Poisson's law, $d^2\phi(z)/dz^2=4\pi n(z)e/\epsilon$, where $\phi(z)$ is the electrostatic potential, $n(z)$ is the 3D electron density in the well, e is the electronic charge, and ϵ is the static dielectric constant. We choose z so that the well extends from $z=0$ to $z=w$. The parabolic variation of the band edge $V_b(z)=4\Delta_1(z-w/2)^2/w^2$ mimics a uniform 3D positive charge distribution of density

$$n_+ = 2\Delta_1\epsilon/\pi e^2 w^2,$$

which the electrons in the well attempt to screen. We speak of a well being full when the total sheet density n_s of electrons is sufficient to completely screen the fictitious positive charge, i.e., when $n_s=n_+w$. We expect a less than full well with a fractional occupation $f=n_s/n_+w < 1$ will have an electronic density profile $n(z)$ which is roughly constant and close to n_+ over a width approximately $w_e = fw$ about the center of the well, as shown in

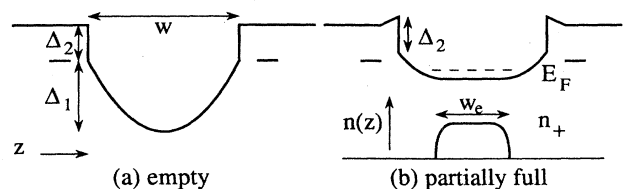


FIG. 1. Schematic illustration of the conduction-band edge in (a) an empty well and (b) a partially full well.

Fig. 1(b). Thus the well acts to create a dense, spatially uniform electron gas of constant density and variable width, with a uniform positive background simulated by the parabolic well. The absence of ionized donors from the well results in a greatly enhanced low-temperature electronic mobility, measured³⁻⁵ to be as high as $\mu = 2.5 \times 10^5 \text{ cm}^2/\text{V sec}$.

In the quantum-mechanical picture, the charge density $-en(z)$ is built up from a superposition of wave functions for the different electric subbands of the well. Ignoring possible collective states,¹ the energy of the electron gas in a given subband i is the sum of the energy for motion in the x - y plane and the self-consistent energy level E_i . The energy levels E_i are expected to be harmonic-oscillator-like when $f \ll 1$ and approach a square-well spectrum $E_i = E_0 i^2$, where $E_0 \propto 1/w_s^2$ is the ground-state energy of a square well of width w_s , approximately equal to the width of the electron layer, as f approaches 1. As the well is filled with electrons³⁻⁵ the Fermi level $E_F - E_1$ remains relatively constant, corresponding to constant density; the energy spacing of the subbands decreases with the increased width of the electron layer, and the number of occupied subbands increases.

The dielectric constant and effective mass have a small quadratic variation across the well from the change in Al concentration. For this calculation, we have taken both to be constant and equal to their average over the well, so that $\epsilon = 12.87$ and $m^* = 0.0753m_e$, where m_e is the bare electron mass. With this choice of ϵ and m^* , and $\Delta_1 = 155 \text{ meV}$ and $w = 4000 \text{ \AA}$ as given above, the design density is $n_+ = 5.5 \times 10^{15} \text{ cm}^{-3}$. In order to avoid the computational difficulties associated with an abrupt change in band-edge potential, the barrier height Δ_2 at the edge of the well has been taken to be infinite in our calculation. This approximation is expected to be reasonable, because the relevant electronic energies are small compared to Δ_2 . For example, the density n_+ above corresponds to a 3D Fermi energy $E_F - E_1 \cong 1.5 \text{ meV}$. Moreover, the electron density falls off rapidly beyond a distance $w_e/2$ from the well center, so the requirement that $n(z)$ vanish in the barrier should be reasonable for $f < 0.8$.

Following a procedure similar to those used for GaAs/Al_xGa_{1-x}As heterojunctions,⁷ the envelope function $\xi_i(z)$ of electrons in the i th subband is assumed to satisfy the Schrödinger equation:

$$-\frac{\hbar^2}{2m^*} \frac{d^2}{dz^2} \xi_i(z) + V(z)\xi_i(z) = E_i \xi_i(z), \quad (1)$$

where E_i is the energy of the bottom of the i th subband and $V(z)$ is the total self-consistent potential. The potential $V(z)$ can be expressed as

$$V(z) = V_b(z) + V_h(z) + V_{xc}(z), \quad (2)$$

where $V_b(z)$ is the parabolic band-edge potential described earlier, $V_h(z)$ is the electrostatic potential of the electron gas, and $V_{xc}(z)$ is the exchange-correlation potential in the Hohenberg-Kohn-Sham local-density-functional approximation. The electrostatic potential is given by

$$V_h(z) = -\frac{2\pi e^2}{\epsilon} \int_0^w n(z') |z - z'| dz'. \quad (3)$$

The electron-density profile in the well $n(z)$ is

$$n(z) = \sum_i n_i |\xi_i(z)|^2, \quad (4)$$

where the sheet density n_i in the i th subband is

$$n_i = m^*(E_F - E_i)/\pi\hbar^2, \quad (5)$$

and E_F is the Fermi energy. The form of the exchange-correlation potential which we chose is one suggested by Hedin and Lundqvist⁸ and used by Stern and Das Sarma in an investigation of GaAs/Al_xGa_{1-x}As heterojunctions:⁷

$$V_{xc}(z) = -[1 + 0.7734x \ln(1 + x^{-1})](2/\pi\alpha r_s) \text{ Ry}^*, \quad (6)$$

Here $\alpha = (4/9\pi)^{1/3}$, and the unit of energy is the effective Rydberg, $1 \text{ Ry}^* \equiv e^2/2\epsilon a^*$, where a^* is the Bohr radius in the well,

$$a^* = \frac{\epsilon\hbar^2}{m^*e^2}. \quad (7)$$

The z dependence of $V_{xc}(z)$ lies in $x = r_s/21$ and $r_s \equiv r_s(z)$:

$$r_s(z) = \left[\frac{4}{3} \pi (a^*)^3 n(z) \right]^{-1/3}. \quad (8)$$

V_{xc} is typically $\cong 2.4 \text{ meV}$ in the electron layer for our calculation. As is standard in these calculations, we have identified the eigenvalues E_i and envelope functions $\xi_i(z)$ with the true subband energies and wave functions, even though the local-density-functional approximation guarantees correct results only for the many-body ground-state energy. We have also ignored image-potential interactions due to the dielectric discontinuity at the well edge, since the change in dielectric constant is small, on the order of 3%.

III. RESULTS

The computed electron density $n(z)$ is shown in Figs. 2(a)–2(d) as a function of position in a 4000- \AA well with $\Delta_1 = 155 \text{ meV}$, $\epsilon = 12.87$, and $m^* = 0.0753m_e$ for four increasing values of total sheet density n_s . Also shown are the contribution to the total density from each subband $n_i |\xi_i(z)|^2$ when more than one subband is occupied and the total self-consistent potential $V(z)$ including band edge, electrostatic, and exchange-correlation terms. For w , Δ_1 , ϵ , and m^* as above, the 3D design density is $n_+ = 5.5 \times 10^{15} \text{ cm}^{-3}$, so that a full well will have the sheet density $n_s = 2.2 \times 10^{11} \text{ cm}^{-2}$. The four choices of n_s here correspond to fractional fillings of $f = n_s/n_+ w = 0.11$ in Fig. 2(a), $f = 0.26$ in Fig. 2(b), $f = 0.465$ in Fig. 2(c), and $f = 0.59$ in Fig. 2(d).

When only one subband is occupied [Fig. 2(a)], the density profile is sharply peaked. The total potential is narrow and not noticeably flattened, with a minimum lying at the center of the well. As the well fills and more subbands become occupied, the profile broadens and flattens over the occupied portion of the well. The total den-

sity remains close to n_+ over a width approximately $w_e = fw$, but with ripples on the order of 10% of n_+ above and below the average. The potential flattens over the same width w_e and its minimum has moved away from the center of the well for $n_s > 0.57 \times 10^{11} \text{ cm}^{-2}$ [Fig. 2(b)]. The number of ripples generally equals the number of substantially occupied subbands, and the overall shape of the density profile is reminiscent of the sum of the first few terms in a Fourier expansion of a square wave, although different in detail.

The width of the self-consistent electron-density profiles in Figs. 2(a)–2(d) clearly becomes broader as n_s increases; to quantify the width so that we can compare it with the simple picture presented in Sec. II, we have defined a measure of the width Δz from the second moment of $n(z)$:

$$(\Delta z)^2 = \frac{12}{n_s} \int_0^w \left[z - \frac{w}{2} \right]^2 n(z) dz, \quad (9)$$

where we know from symmetry that $w/2$ is the average of z over the well. Considering an “ideal” density profile to be equal to n_+ over a distance w_e about the center of the well and zero elsewhere, we have that for such a profile $\Delta z = w_e \propto n_s$. The self-consistent values of Δz are plotted with w_e versus n_s in Fig. 3. For low values of n_s , Δz is approximately constant $\Delta z \approx 500 \text{ \AA}$, significantly larger than the ideal value w_e , but for $n_s > 0.35 \times 10^{11} \text{ cm}^{-2}$ ($f > 0.16$) the two are almost identical. The linearity of Δz in n_s for $n_s > 0.40 \times 10^{11} \text{ cm}^{-2}$ (approximately the value of n_s at which the second subband begins to fill) is very striking.

In Fig. 4 we compare three density profiles $n(z)$ for $n_s = 0.77 \times 10^{11} \text{ cm}^{-2}$ ($f = 0.35$, three occupied subbands). Two profiles were calculated self-consistently with and without $V_{xc}(z)$, respectively. The density profile in the absence of the exchange-correlation potential shows noticeably less ripple and is slightly broader than the profile with the potential turned on: $\Delta z \approx 1470 \text{ \AA}$ without $V_{xc}(z)$, while $\Delta z \approx 1410 \text{ \AA}$ with $V_{xc}(z)$. The lowest 5 meV of the total potentials for the self-consistent profiles are also shown in Fig. 4. Without $V_{xc}(z)$, the potential rises less rapidly, and its minimum lies at the center of the well.

The third profile shown in Fig. 4 was calculated using Eqs. (4) and (5) for the same sheet density n_s , but for sinusoidal wave functions and square-well energy levels $E_i = \hbar^2 \pi^2 i^2 / 2m^* w_s^2$. Here w_s is a width generally not equal to w_e , as in the simple model discussed in Sec. II, and is chosen by fitting the energy spectrum as discussed below. The sine-based profile is very similar to the self-consistent profile, except for slightly less pronounced ripple. However, this level of agreement may be an accidental consequence of this choice of parameters.

In Fig. 5 we show the Fermi level $E_F - E_1$ and subband separations $E_i - E_1$ as a function of n_s for the full self-consistent calculation. When only one subband is occupied, the Fermi level rises linearly with n_s , as it must in a two-dimensional system. As each higher subband begins to fill, a discontinuity in slope in $E_F - E_1$ occurs, and the Fermi level rises more slowly. For $n_s > 1.0 \times 10^{11} \text{ cm}^{-2}$,

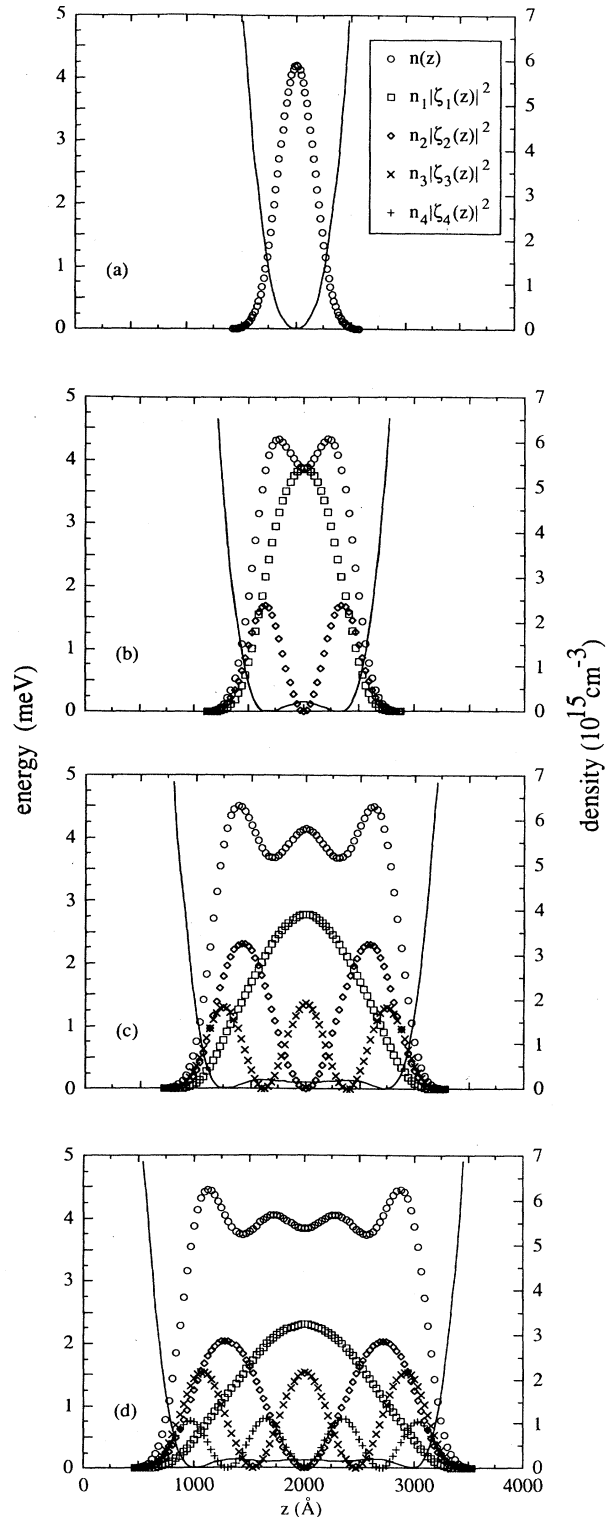


FIG. 2. Electron density, subbands weighted for relative occupation (points), and total potential (solid line) as a function of position in the well for four values of n_s : (a) $n_s = 0.24 \times 10^{11} \text{ cm}^{-2}$, (b) $n_s = 0.57 \times 10^{11} \text{ cm}^{-2}$, (c) $n_s = 1.0 \times 10^{11} \text{ cm}^{-2}$, and (d) $n_s = 1.3 \times 10^{11} \text{ cm}^{-2}$. The curves represented by points are not experimental results, but discrete theoretical values calculated using a finite basis set.

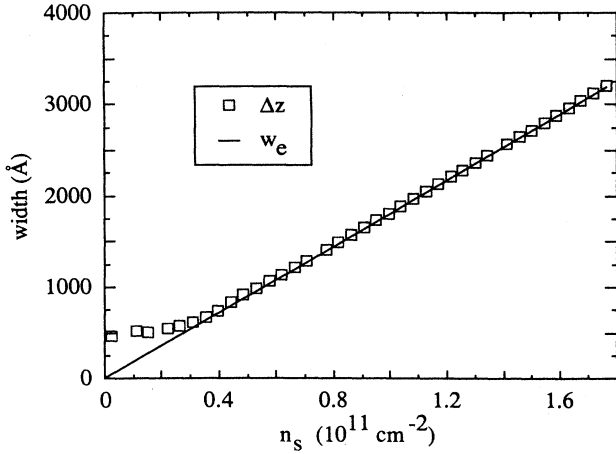


FIG. 3. Calculated actual width Δz and the nominal electron-gas width w_e vs n_s . A completely full well corresponds to $N_s = 2.2 \times 10^{11} \text{ cm}^{-2}$.

the Fermi level is nearly constant, as for a 3D electron gas, rising only from $E_F - E_1 = 1.45 \text{ meV}$ at $n_s = 1.0 \times 10^{11} \text{ cm}^{-2}$ to $E_F - E_1 = 1.50 \text{ meV}$ at $n_s = 1.8 \times 10^{11} \text{ cm}^{-2}$. The value near which it is fixed is the 3D Fermi level $E_F - E_1 = 1.5 \text{ meV}$ calculated from n_+ alone, as in the simple picture described in Sec. II. As expected the subband separations drop rapidly with increasing n_s as the electron layer becomes wider.

In Fig. 6 we show the separations between adjacent subbands $E_{i+1} - E_i$ plotted versus the filling fraction f for $i = 1-5$. For small values of f , the separations are almost independent of i and f (and therefore n_s), as expected for a simple harmonic oscillator: For $f = 0.01$, $E_2 - E_1 = 2.96 \text{ meV}$ and $E_6 - E_5 = 2.80 \text{ meV}$, in excellent

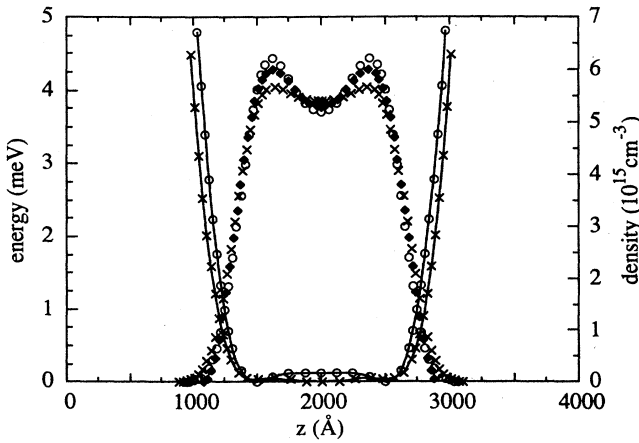


FIG. 4. Electron density and total potential for self-consistent calculations with (\circ) and without (\times) the exchange-correlation potential for $n_s = 0.77 \times 10^{11} \text{ cm}^{-2}$. The third density profile (\blacklozenge) was calculated for the same value of n_s assuming the subbands and energies were those of a square well of width w_e (see text).

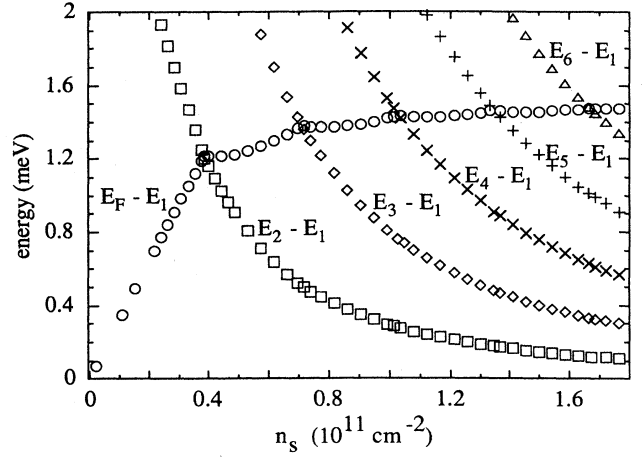


FIG. 5. Theoretically calculated Fermi-level $E_F - E_1$ and energy-level separations $E_i - E_1$ vs n_s .

agreement with the expected separation for a simple harmonic oscillator $\hbar(8\Delta_1/m^*w^2)^{1/2} = 2.80 \text{ meV}$. However, as the filling fraction increases above $f = 0.10$, the subband separations begin to vary with index i and fall rapidly with f . When the well is nearly full and f approaches 1, the subband separations fall approximately as $1/f^2$, as for the simple picture of a square well of variable width discussed in Sec. II. For comparison, the separation of the first two energy levels $E_2 - E_1 \propto 1/f^2$ for a square well of width equal to the nominal width of the electron layer $w_e = fw$ is also shown in Fig. 6 as the solid line. As shown the energy separation from this simple model is larger and falls somewhat faster with f than the results of the self-consistent calculations; we return to this point below. The subband separations $E_{i+1} - E_i$ from the self-consistent calculation increase with i in an approximately linear way for $f > 0.60$, as for square-well energy levels $E_i \propto i^2/w_e^2$.

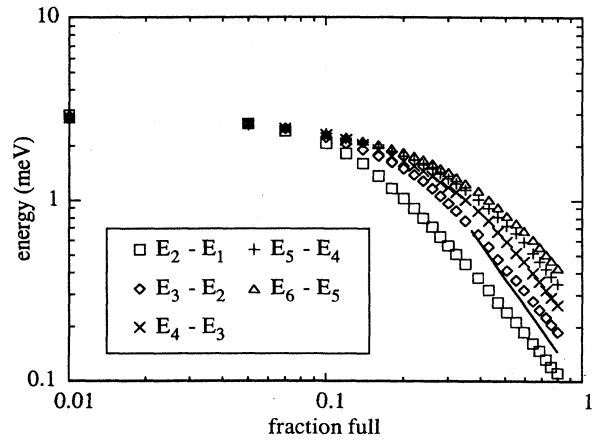


FIG. 6. Calculated subband separations $E_{i+1} - E_i$ for $i = 1-5$ vs n_s . The solid line is the separation of the lowest two energy levels in a square well of width w_e .

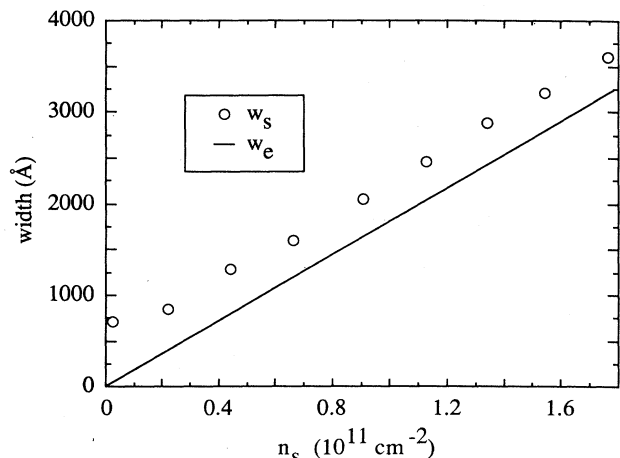


FIG. 7. Calculated effective square-well width w_s and nominal electron-gas width w_e vs n_s .

The calculated separations between occupied energy subbands can be fit very closely by a square-well spectrum; this fit can be used to define an effective square-well width w_s . We made such fits using the separations $E_i - E_1$ for all E_i up to and including the energy of the first unoccupied subband, and present the results as a function of n_s in Fig. 7. For $n_s > 0.2 \times 10^{11} \text{ cm}^{-2}$ the effective well width w_s is linear in n_s but greater than the nominal electron gas width w_e by a fixed amount $\cong 400 \text{ \AA}$, which is independent of n_s . Thus the energy separations are smaller than one would obtain by setting $w_s = w_e$, as shown in Fig. 6 for $E_2 - E_1$. Because the actual width of the electron layer Δz closely approximates the ideal width w_e , the effective square-well width w_s must be larger to provide space for the wave functions to approach zero. The sine density profile $n(z)$ in Fig. 4 was calculated using an effective width w_s chosen by the procedure just described; clearly a square-well model provides a good approximation to self-consistent density profiles and energies if the effective width w_s is chosen correctly.

In Fig. 8 we show the fractional occupation of each subband $f_i = n_i / n_s$ as a function of the sheet density n_s . As shown, for $n_s > 0.45 \times 10^{11} \text{ cm}^{-2}$ ($f > 0.20$) a significant fraction of the electrons are not located in the lowest subband. Consequently the electronic transport

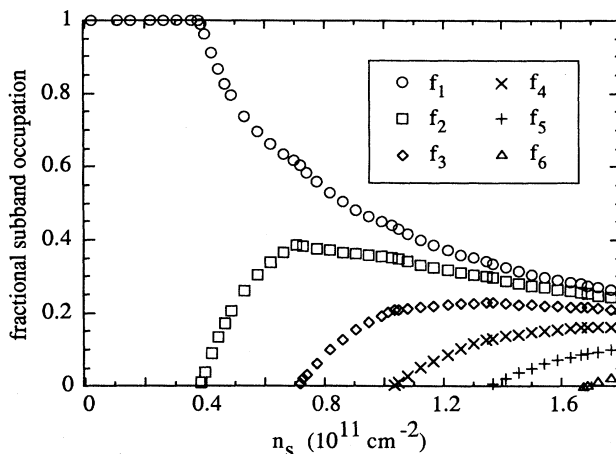


FIG. 8. Calculated fractional subband occupancies f_i vs n_s for $i = 1-6$.

properties could be controlled to an appreciable extent by properties of the higher subbands.

IV. CONCLUSIONS

Parabolic quantum wells were conceived² on the basis of semiclassical and classical arguments. While we have made a number of simplifying approximations in our calculations, it seems clear that a full quantum-mechanical treatment of energy levels in these wells supports the original arguments. The wells hold an electron gas with fixed 3D density approximately equal to the design density n_+ over a variable width proportional to the total sheet density n_s . The Fermi level is found to be approximately independent of n_s and close to the 3D Fermi level. The spacing between energy levels decreases as n_s increases, and the level separations come to approximate those of a square well of variable width as the well becomes full.

ACKNOWLEDGMENTS

We thank D. Vanderbilt and E. G. Gwinn for useful comments and discussions. One of us (A.J.R.) acknowledges support from the National Science Foundation. This work was supported in part by National Science Foundation Grant No. DMR-88-17309.

¹Reviewed in B. I. Halperin, *Jpn. J. Appl. Phys.* **26**, Suppl. 26-3, 1913 (1987).

²M. Sundaram, A. C. Gossard, J. H. English, and R. M. Westervelt, *Superlatt. Microstruct.* **4**, 683 (1988).

³E. G. Gwinn, P. F. Hopkins, A. J. Rimberg, R. M. Westervelt, M. Sundaram, and A. C. Gossard, in *High Magnetic Fields in Semiconductor Physics II*, edited by G. Landwehr (Springer-Verlag, New York, in press).

⁴E. G. Gwinn, R. M. Westervelt, P. F. Hopkins, A. J. Rimberg,

M. Sundaram, and A. C. Gossard, *Superlatt. Microstruct.* **6**, 95 (1989).

⁵E. G. Gwinn, R. M. Westervelt, P. F. Hopkins, A. J. Rimberg, M. Sundaram, and A. C. Gossard, *Phys. Rev. B* **39**, 6260 (1989).

⁶M. Shayegan, T. Sajoto, M. Santos, and C. Silvestre, *Appl. Phys. Lett.* (to be published).

⁷F. Stern and S. Das Sarma, *Phys. Rev. B* **30**, 840 (1984).

⁸L. Hedin and B. I. Lundqvist, *J. Phys. C* **4**, 2064 (1971).